Proc. Natl. Acad. Sci. USA
Vol. 95, pp. 8502–8507, July 1998
Biochemistry

The allosteric mechanism of the chaperonin GroEL: A dynamic analysis

JIANPENG MA* AND MARTIN KARPLUS*†‡

*Department of Chemistry and Chemical Biology, Harvard University, Cambridge, MA 02138; and †Laboratoire de Chimie Biophysique, Institut le Bel, Universite Louis Pasteur, 67000 Strasbourg, France

Contributed by Martin Karplus, May 4, 1998

ABSTRACT **Normal mode calculations on individual subunits and a multisubunit construct are used to analyze the structural transitions that occur during the GroEL cycle. The normal modes demonstrate that the specific displacements of the domains (hinge bending, twisting) observed in the structural studies arise from the intrinsic flexibility of the subunits. The allosteric mechanism (positive cooperativity within a ring, negative cooperativity between rings) is shown to be based on coupled tertiary structural changes, rather than the quaternary transition found in classic allosteric proteins. The results unify static structural data from x-ray crystallography and cryoelectron microscopy with functional measurements of binding and cooperativity.**

The molecular chaperonin GroEL mediates protein folding in the bacterial cell (1–7). GroEL consists of a double-ringed cylinder with each ring composed of seven identical subunits. There is a large central cavity in which the polypeptide chain is sequestered during the folding process. The change of shape of the cavity during the GroEL cycle of activity is believed to play an important role in folding. It is coupled to ATP binding, to hydrolysis, and to interactions with the cochaperonin GroES. Each subunit has a site for binding and hydrolysis of ATP, and there is positive cooperativity for binding and hydrolysis in the same ring and negative cooperativity between the two rings (3, 8–10). Based on cryoelectron microscopy (11–13), it was concluded that large, structural changes occur in the subunits during the GroEL cycle. Critical information on the details of the conformational change has been obtained recently from the crystal structure of the asymmetric complex GroEL-GroES-$(ADP)_7$ (14) and its comparison with earlier structures (15–17).

Because the available structural data are based on comparisons of stable states of GroEL, it is important to complement them by dynamical studies of the transitions involved. The present paper employs normal mode analysis for this purpose. Normal mode studies of lysozyme (18), hexokinase (19), and citrate synthase (20), as well as of multisubunit proteins [hemoglobin (21) and ATCase (22)], have been used to interpret the structural changes that occur on ligand binding (23). The results indicate that the structures of certain proteins have evolved so that their intrinsic flexibility facilitates the conformational changes required for function. Given the multidomain structure of the subunits and the multisubunit structure of the GroEL complex, a normal mode analysis is ideally suited for providing a link between the observed structural changes and the molecular properties involved.

In this paper we describe normal mode calculations for a single GroEL subunit with and without the effector ATP and of a three-equatorial-domain construct (one in the cis ring and two in the trans ring). The results are used to develop an allosteric model for positive cooperativity within a ring and negative cooperativity between the rings.

METHODS

Normal mode calculations were performed by using standard techniques (23, 24). All of the structures were energy-minimized by 1,000 steps of the steepest descent method followed by a few thousand steps of the Adapted Basis Newton Raphsen method (25); the minimizations were terminated when the rms energy gradient had been reduced to 10^{-7} kcal/mol-Å. Only the low-frequency modes that give rise to the largest displacements are considered. They provide details concerning the important interdomain motions and displacements of flexible elements within a domain. Higher-frequency modes are of less interest because they are composed of relatively small localized motions (22, 26). The normal modes results shown in the figures are normalized to an average rms displacement of 3 Å in the positive and negative directions, relative to the minimized structure used for the calculations.

The normal-mode calculations were performed with the VIBRAN module in the CHARMM program (24, 25). An empirical energy function based on the polar hydrogen model (CHARMM19) was employed, and a distant dependent dielectric constant was used to provide approximate solvent shielding of distant charges.

RESULTS

Schematic representations of the GroEL subunit from two different views are shown in Fig. 1. It is evident from Fig. 1*a* that the subunit is composed of three domains (equatorial, intermediate, and apical) connected by two hinge regions. Although the hinge regions are defined clearly in the schematic main-chain representations, space-filling models including all heavy atoms show that there are many contacts between the domains (see, for example, figure 3d of ref. 15) and that their relative motions must involve complex interactions. The normal mode calculations elucidate the nature of the allowed large amplitude motions of the three domains; of particular importance is the inherent directionality of the motions, which cannot be determined from the structures alone.

Inherent Motions of the GroEL Subunit. Fig. 2*a* shows the lowest-frequency mode (1.18 cm^{-1}) of the GroEL subunit. The apical and intermediate domains move essentially like a rigid body relative to the equatorial domain, corresponding to a "hinge-bending" mode with respect to hinge 1 (see Fig. 1). There is an upward displacement of the apical domain, accompanied by a shift of the intermediate domain. The apical and intermediate domains rotate together with respect to the equatorial domain; i.e., if one looks down from the top, this mode involves a significant "twist" of the two domains about hinge 1 relative to the equatorial domain. That the hinge is localized in Gly-410 of one strand and Pro-137 of the other

The publication costs of this article were defrayed in part by page charge payment. This article must therefore be hereby marked "*advertisement*" in accordance with 18 U.S.C. §1734 solely to indicate this fact.

‡To whom reprint requests should be addressed. e-mail: marci@tammy.harvard.edu.

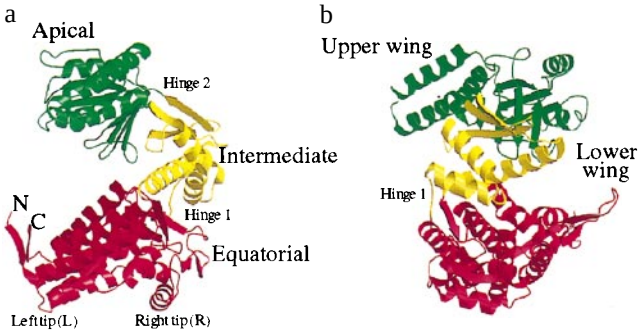

FIG. 1. Schematic representations of the subunit of GroEL from the structure by Braig *et al*. (15). The apical (green), intermediate (yellow), and equatorial domains (red) are evident. (*a*) View chosen to show the hinge regions and the two "tips" of the equatorial domain that make contact with subunits in the other ring of GroEL. It corresponds to the orientation of a subunit on the upper ring viewed from the front of the GroEL molecule; see, for example, figure 9d in Roseman *et al*. (12). The β-strands S5 and S13 referred to in the text are the two top strands in the intermediate domain. (*b*) View generated by a 90° clockwise rotation of *a* around a vertical axis. Two regions (labeled as "wings") by which the GroEL subunit makes contacts with its neighboring subunits are indicated. Labels of secondary structural elements in text and figures follow Braig *et al*. (numbers for helices) (16) and Xu *et al*. (letters for helices) (14). The drawings in *Left* and *Right* are made with MOLSCRIPT (45) and RASTER 3D (46).

strand connecting the two domains emerges directly from the normal-mode calculations and is in accord with the conclusion based on a comparison of x-ray structures (14). Because the two connecting strands are located asymmetrically (i.e., they are in the "front" in Fig. 1*a* and to the "left" in Fig. 1*b*), the twisting displacement of the intermediate domain is best characterized as a "folding motion," which moves it downward to cover the ATP-binding site of the equatorial domain while simultaneously rotating the apical domain. The motion corresponding to this mode leads to a structural change similar to that described by Xu *et al*. (14), as can be seen by comparing their figures 2b and 2d with Fig. 2*b* of the present paper. Helix 13 (H13 or M) in the intermediate domain rotates by a large angle and makes several new contacts with the equatorial domain. The two other helices, H6(F) and H7(G), and the three-stranded β-sheet of the intermediate domain also reorient significantly. A new contact between H13(M) and the stem loop observed in the x-ray structure requires motion of the stem loop, which does not occur in this mode but is clearly seen in mode 4 (see below).

There are several other low-frequency modes that involve significant displacements of the apical domain. The second mode (1.38 cm^{-1}) is dominated by an anticorrelated twisting motion around hinge 1 and 2; i.e., the apical domain rotates in one direction and the intermediate domain in the other (not shown). The third mode (1.76 cm^{-1}) also involves motion with respect to both hinges (not shown). However, in contrast to the second mode, there is an upward displacement of the apical domain about hinge 1 (similar to that in mode 1) and a rotation about hinge 2. The apical domain rotates around an axis parallel to the plane formed by β-strands S5–S13 near hinge 2 (see Fig. 1 legend). Hinge 2 is not as localized as hinge 1, but involves some twisting of the intermediate domain β-strands in the neighborhood of the apical domain. Because of the orientation of the ends of strand S5 and S13 at the contact between the apical and intermediate domain, the hinge is found to be more flexible for twisting around such an axis than for bending in the plane.

The twist of the apical domain inferred from the cryoelectron microscopy and x-ray results can be obtained by combining the calculated motions from several low-frequency modes about hinge 1 and 2. However, superposition of the same modes with appropriate phases still leads to only partial opening of the apical domain, relative to that observed by Xu *et al*. (14). In fact, the normal-mode displacement is much closer to that shown in the recent cryoelectron microscopy reconstruction by White *et al.* (27) of GroEL with ATP bound to one of the rings (see their figure 3b). This indicates that the first step in the essential transitions of the GroEL functional cycle involves a displacement of the intermediate domain induced by ATP to cover its binding site in the equatorial domain plus a rotation and small upward motion of the apical domain; the rotation reorients key hydrophobic residues (7) so that they are positioned for the binding of GroES, rather than for interaction with the folding polypeptide chain. This is apparently followed by an additional opening of the apical domain, induced by binding to GroES in the presence of ATP or other nucleotides (12, 13). The importance of the motion about hinge 2 for GroES binding is supported by the result that the mutations of residues of the intermediate domain at the end of the β-strands near hinge 2 reduce the interaction between the GroEL and GroES (28, 29).

To examine the effect of ATP on the dynamics, we have calculated the normal modes of a single subunit with bound ATP. This is of particular interest because of the kinetic analysis of Jackson *et al*. (10), which separated faster ATP binding from the slower hydrolysis, and the recent study by Rye *et al*. (30) of a hydrolysis-defective mutant, which demonstrated that the normal conformational transitions, including GroES binding, occur in the absence of hydrolysis; see also Hayer-Hart *et al*. (31), who showed that ATP hydrolysis is not necessary for certain portions of the GroEL cycle. The ATP[γS]-bound structure was used for the calculations (17); it is very similar to the free structure except for small changes in the equatorial domain, possibly because the ligand is symmetrically bound to the subunits of both rings (14, 17). The normal-mode results show that there is a significant difference in the overall flexibility of the domains between the free and ATP-bound structures. Room temperature rms fluctuations calculated from the sum over the 10 lowest modes that dominate the large-scale motions (26) show that the equatorial domain is more rigid (smaller rms fluctuations on average) and both the intermediate and apical domain are more flexible (larger rms fluctuations on average) in the ATP-bound structure. The greatest rigidification occurs for H4(D), which would make it an effective fulcrum for transmitting information (11, 12); H4(D) was observed to have very low thermal factors in the GroEL-GroES-$(ADP)_7$ complex (P. Sigler, personal communication). The lowest-frequency mode of the subunit with bound ATP [frequency 1.28 cm^{-1} (not shown)] is similar to that in the free subunit except that the apical domain moves upward more than in the free subunit; the resulting displacement is still significantly smaller than that observed by Xu *et al*. (14), confirming the GroES binding is required to obtain the fully open structure. Certain intradomain motions that may be involved in the allosteric mechanism appear in a single mode of the liganded subunit, whereas they are distributed between different modes of the free subunit; they are described below.

Allosteric Mechanism. An essential question concerning GroEL is the origin of the cooperativity in the binding and hydrolysis of ATP (8). Hydrolysis data have been fitted (32, 33) by a model having two different quaternary structures for each ring [T and R states, in accord with the Monod, Wyman, and Changeaux (MWC) model (34)] that combine to yield TT, TR, and RR states for the two rings. The description of the cooperativity within a ring as involving a quaternary transition corresponds to that for classic allosteric proteins such as hemoglobin (35). However, the present analysis suggests that, although the MWC model can be used to fit the functional data, the essence of the intraring allosteric transition in GroEL is significantly different. In hemoglobin, only relatively small, though important,

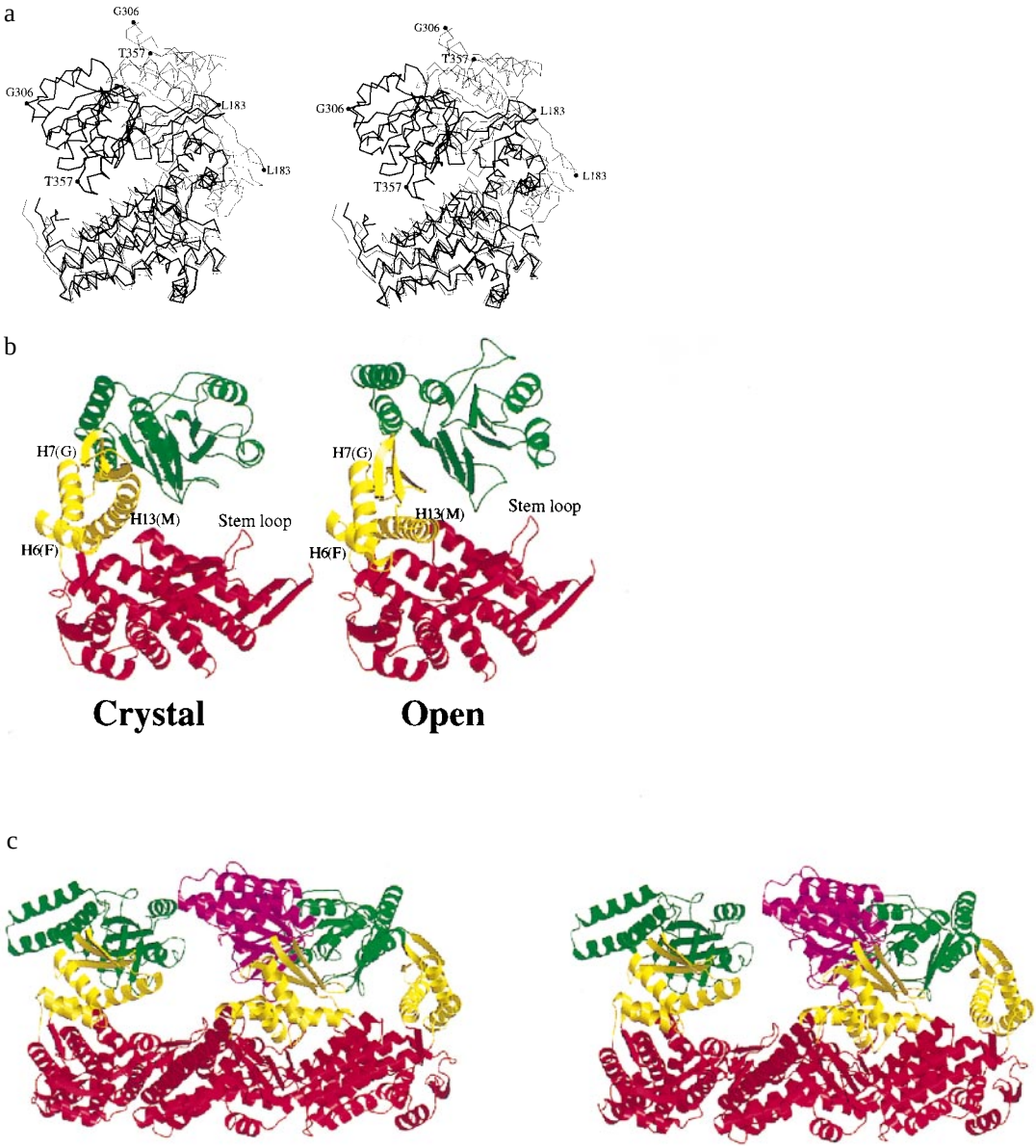

FIG. 2. (*a*) Stereo diagram of the lowest frequency mode of a GroEL subunit with the same orientation as in Fig. 1*a*. The two structures correspond to equal positive (light lines) and negative (dark lines) displacements relative to the minimized structure x-ray structure (15, 16); the two structures are superimposed by optimizing the fits of the equatorial domains to show the displacements of the intermediate and apical domains. Certain residues are labeled to make it easier to follow the motion; they are G306 and T357 in the apical domain and L183 in the intermediate domain. (*b*) Representation of the same mode, oriented for comparison with figure 2d in Xu *et al*. (14). The left-hand figure is the x-ray structure of free GroEL (15), and the right-hand figure is the positive end point of the normal mode. (*c*) Stereoview of three adjacent subunits in the cis ring. The middle subunit is in the open structure predicted by the normal mode analysis (*a*), and the subunits on the two sides have the closed conformation (15, 16). The middle subunit was positioned by superposing its equatorial domain with that of the crystal structure. The apical domain of the middle subunit is shown in purple to differentiate it from the apical domain of the subunit on the right. The drawings were made with MOLSCRIPT (45) and RASTER 3D (46).

tertiary structural changes in each subunit result on ligand binding and it is the large relative displacements of the subunits that produce the quaternary transition from the T to the R structure (35–37). In GroEL, by contrast, the tertiary structural changes involving hinged domain motions within a subunit are very large and there is no evidence for a quaternary transition involving significant relative motions of the subunits. Thus, the intraring allosteric mechanism is more correctly described in terms of coupled tertiary structural changes. As we indicate below, the tertiary transitions appear to be concerted and therefore can be encompassed in the MWC model. In what follows we outline a mechanism for the cooperative transitions involved in ATP binding to GroEL (10); the cooperativity in ATP hydrolysis (8, 38) appears to be closely related, but not enough is known about the reaction mechanism to elucidate the effects of the structural changes. The study of ATP binding, *per se*, is justified by the measurements of Jackson *et al*. (10) and Rye *et al*. (30), as described above.

The dominant tertiary structures of each subunit correspond to a **t** state (closed, in the absence of ATP), **t′** ("super" closed, in absence of ATP with ATP bound in other ring), and at least two **r** states, **r′** (partly open with ATP bound, in the absence of GroES) and **r″** (fully open with ATP bound, in the presence of GroES); we use lowercase letters to emphasize that we are considering tertiary, rather than quaternary, structural changes. Additional tertiary structures may have to be introduced as more details become available (e.g., ADP- vs. ATP-bound structures (12, 13), but they are expected to be similar

to one of the four considered here. Measurements have shown that at low concentrations, ATP binds weakly to GroEL in a noncooperative manner (10). We identify the weak binding with binding to the **t** state. This is in accord with the results for cross-linked GroEL, which demonstrated ATP binding to a closed conformation (39). At higher ATP concentrations, the binding constant for ATP increases by approximately 400-fold. This increase in binding affinity was shown to be accompanied by a conformational change via a fluorescence assay, and the measured cooperative binding curve for ATP was fitted to a Hill plot with a Hill constant **n** equal to 4 (10). We identify the increase in binding constant with the subunit conformational change from **t** to **r′**. The normal mode results suggest that **r′** is the structure shown in Fig. 2 with the partly open apical domain position and the ATP-binding site covered by the intermediate domain.

The structural change of a subunit involved in the transitions from **t** to **r′** cannot take place in the presence of two neighboring subunits in the unliganded (**t**) state. There are large, repulsive van der Waals interactions between the subunits, particularly between the apical domain of the open (**r′**) subunit and its closed (**t**) neighbor on the right (see Fig. 2*c*). This appears to be an important source of the cooperativity because the steric clashes are resolved if all the subunits shift simultaneously to the **r′** structure. The normal mode results and experiments also suggest that, in addition to the large-scale-domain motions, intradomain structural changes and specific interactions are important for cooperativity (see below).

GroES binding requires an additional structural change in all of the subunits (12–14). The increased upward displacement of the apical domain, beyond that found in the normal mode calculation, is identified with the transition from **r′** to **r″**. The binding of GroES is expected to strengthen the coupling of the tertiary structural changes of the individual subunits. Experimentally, the Hill constant **n** for ATP binding increases from 4 to 6 in the presence of GroES (10). This can be ascribed to a change in the allosteric constant **L** of the MWC model, if the binding constants of the **r′** and **r″** states are the same.

Interactions between the two rings of GroEL lead to negative cooperativity in the binding and hydrolysis of ATP, in the absence, as well as in the presence of GroES; e.g., the cis ring binds ATP at relatively low concentrations and a much higher concentration of ATP is required to obtain binding to both rings, as shown by functional (38) and structural (12, 13) studies. The only contacts between the rings involve the equatorial domains. Motion of these domains on the binding of ATP to the cis ring in the absence of GroES [i.e., the transition $(\mathbf{t})_7$ to $(\mathbf{r}')_7$] is such as to inhibit the $(\mathbf{t})_7$ to $(\mathbf{r}')_7$ transition in the trans ring by stabilizing a "super" closed state, $(\mathbf{t}')_7$ in the trans ring. If the bound ATP is hydrolyzed to ADP in the cis ring and ATP binds to the trans ring, the inverse transition appears to be induced (30); i.e., $(\mathbf{t}')_7$ changes to $(\mathbf{r}')_7$ in the trans ring and $(\mathbf{r}')_7$ changes to $(\mathbf{t})_7$ or $(\mathbf{t}')_7$ in the cis ring with release of ADP. This sequence describes the essential elements of a GroEL structural cycle in the absence of GroES. When GroES is present, corresponding behavior, with the **r″** subunit structure contributing as described above, is predicted. In what follows, we discuss some specific features of the normal-mode motions that may be involved in the allosteric mechanism.

Intraring Communication. In addition to the distributed steric repulsions that contribute to the cooperative subunit shift to the open structure (see above), there are specific intersubunit interactions that result from the tertiary structural changes induced by ATP binding. One intersubunit contact consists of the S2/S3 β-hairpin (stem loop), which extends outward from the equatorial domain (the "lower wing" in Fig. 1*b*) and forms a parallel β-sheet with segments S18 and S1 of the equatorial domain of the neighboring subunit. Because a deletion mutant including residue 521 in S18 prevents assembly of the GroEL ring (15), this interaction appears to be essential for stability and it is likely to be important in the allosteric mechanism. The stem loop is one of the structural elements that undergoes a significant change on the binding of ATP[γS] to GroEL (17), and a similar change was observed in the GroEL-GroES-$(ADP)_7$ complex (14). A second intersubunit contact involves the apical domain of one subunit and the intermediate domain of its left-handed neighboring subunit (looking in the direction corresponding to Fig. 1*a*). There is a protrusion of the apical domain ("upper wing" in Fig. 1*b*) formed by H11(K) and H12(L) and the turn connecting them. This is a region where the **t** to **r′** transition results in steric clashes with the neighboring subunit. Arg-197, which is located in the end of S6 in the apical domain below the upper wing, makes a salt bridge with Glu-386 at the N-terminal end of H13(M) of the intermediate domain in the left-handed neighboring subunit. The mutation of Arg-197 → Ala has been shown to disrupt the positive cooperativity among the subunits within a ring (33). Also, a recent cryo-electron microscopy study (27) shows that such a mutation results in a loosening of the ring, particularly an "outward" displacement of the apical domains. It is possible, therefore, that the salt bridge is important primarily for the integrity of the structure, which is necessary for the cooperative tertiary structural changes within in a ring.

The low-frequency modes show large displacements of the two wings (Fig. 1*b*). In the structure without the ATP, the lower wing (stem-loop region) moves relative to the rest of the structure in mode 4 (frequency, 1.92 cm^{-1}) (see Fig. 3*a*); the stem-loop motion is similar to that observed in ATP[γS]-bound structure (17) and is required for its interaction with the intermediate domain on ATP binding (see above). In mode 5 (frequency, 2.28 cm^{-1}) the upper wing moves relative to the rest of the apical domain (Fig. 3*b*). The ATP-bound structure has a single mode (mode 4, frequency, 2.44 cm^{-1}) with large amplitude motions of both the lower and the upper wings (Fig. 3*c*). This demonstrates how the presence of ATP can alter the normal modes so as to couple displacements that are likely to be involved in intersubunit communication.

Two types of motions within the equatorial domain are of interest for the cooperative interactions. The first, described above, is that of the β-hairpin ("stem loop") consisting of strands S2 and S3. The lowest-frequency mode of the isolated equatorial domain without ATP (frequency, 2.46 cm^{-1}) shows a significant displacement of this region, corresponding to that illustrated in Fig. 3*a* for the entire subunit. A second structural change involves the ends of helices near Arg-13 (H1), which undergo a twisting motion relative to their other ends near the γ-phosphate-binding site in certain normal modes. This motion is illustrated by the second-lowest mode of the empty equatorial domain (frequency, 3.33 cm^{-1}) shown in Fig. 3*d*. The lowest-frequency mode (frequency, 2.78 cm^{-1}; not shown) of the ATP-bound equatorial domain combines the two motions shown in Fig. 3 *a* and *d*. Because the former motion is involved in intraring interactions of the subunits, whereas the latter could contribute to interring interactions, their coupling in a single mode in the presence of ATP is significant.

Interring Communication. Interactions between the two rings of GroEL lead to negative cooperativity in the binding and hydrolysis of ATP; e.g., the cis ring binds ATP at relatively low concentrations and a much higher concentration of ATP is required to obtain binding to both rings, as shown by functional (38) and structural (12, 13) studies. Because the only contacts between the rings involve the lower portions of equatorial domains, their motions must play the dominant role in the coupling. There are two primary regions of close contact, which are labeled as the two "tips" in Fig. 1*a*. In the lowest normal mode of a single subunit (shown in Fig. 2*a*), which presents the structural transition from **t** to **r′**, there is significant motion of the equatorial domain, as shown in Fig. 4*a*. The opening motion corresponding to Fig. 2*a* leads to a

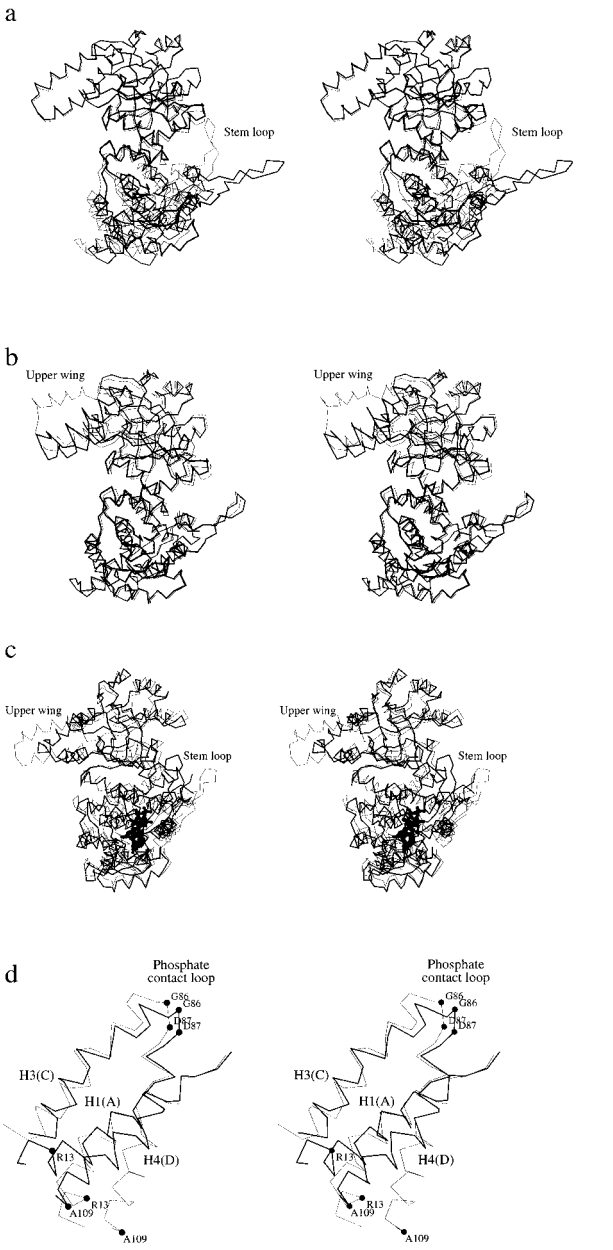

FIG. 3. (*a*) Stereoview of motion corresponding to mode 4 in absence of ATP. (*b*) Stereoview of motion corresponding to mode 5 in absence of ATP. (*c*) Stereoview of motion corresponding to mode 4 in presence of bound ATP. ATP is shown in a ball-and-stick model. (*d*) Stereoview of motion corresponding to mode 2 of the isolated equatorial domain without ATP. The helices with significant twisting motion are shown. The drawings were made with MOLSCRIPT (45).

downward displacement of tip L and relative upward motion of tip R. Several higher-frequency modes (e.g., mode 3) show corresponding displacements of the equatorial domain.

Because each equatorial domain in one ring interacts directly with the two equatorial domains in the other ring, a normal mode calculation was performed for a construct consisting of three equatorial domains (one equatorial domain in the cis ring and two others below it in the trans ring); such a triangular complex forms the minimum interring contact unit of GroEL. Fig. 4*b* shows a low-frequency mode (1.39 cm^{-1}) of the three-domain assembly in the "front" view; i.e., the domain in the cis ring is in approximately the same orientation as Fig. 1*a*. The cis ring domain and the left trans ring domains are related by a dyad axis; the right trans ring domain is related in a corresponding way to a domain in the cis ring (not included).

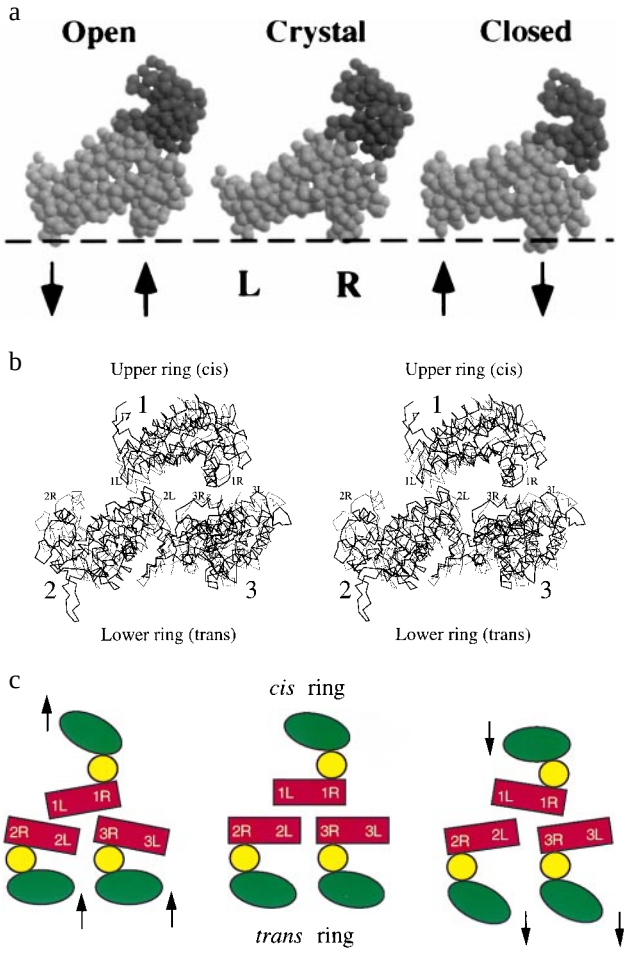

FIG. 4. (*a*) Motion of equatorial domain corresponding to mode 1; only the intermediate and equatorial domains are included for clarity, and a van der Waals sphere representation of the C_α atom is used to show the global motions. The middle image is the minimized subunit; the left and right images correspond to the limiting displacements of the normal mode (see *Methods*). The horizontal line is a schematic representation of the interface between the two rings. Arrows are used to indicate the alternating motion of the equatorial domain with respect to the interface. The view and motion shown are the same as those of the entire subunit in Fig. 2*a*; however, in that figure, the equatorial domain is used as the reference and so does not move. (*b*) Stereoview of motion corresponding to a low-frequency mode of the three-equatorial-domain construct. (*c*) Schematic illustration of coupled subunit motions in the two rings. The arrows represent the direction of the motion of the equatorial domain. Labels 1, 2, and 3 identify the three equatorial domains shown in *b*, and L and R identify the two tips that are the most important contacts between the domains (see Fig. 1*a*). (*a*) Drawn with QUANTA (Molecular Simulations, Waltham, MA). (*b*) Made with MOLSCRIPT (45).

The upper (cis ring) domain undergoes the motion illustrated in Fig. 4*a*. The coupled motion of the trans ring domains is best described by considering the two contact points of each of the equatorial domains (the tips labeled in Fig. 1*a*; see also the schematic Fig. 4*c*). In this mode, 2L (i.e., the tip L of domain 2, even though it is on the right in the figure because of the dyad rotation), which is in contact with 1L, moves in-phase with the cis domain; the tip 3R moves in-phase with 1R in the cis domain. However, 2R and 1L are out-of-phase, while 3L and 1R are in-phase, though the motion of 3L is small.

The resulting interring motions are illustrated in the schematic diagram (Fig. 4*c*), which is based on Fig. 4*b* and the full subunit modes. The left diagram (relative to the middle diagram) illustrates the "closing" of two trans ring subunits as a consequence of the "opening" of the cis ring subunit that is

in contact with them. Such a displacement results in negative cooperativity between the rings; i.e., the displacement of the equatorial domain of the cis ring, which is part of the tertiary structural change from **t** to **r′** or **r″**, leads to inverse displacements of the equatorial domains in the trans ring and increases the energy required for the **t′** to **r′** or **r″** transition in the latter. The major part of the displacement involves overall equatorial domain motion. This is in accord with the observation of Xu *et al*. (14) that in the GroEL-GroES-$(ADP)_7$ structure there is a downward "tilt" of the equatorial domains in the cis ring and a concomitant smaller inverse tilt of the equatorial domains in the trans ring. The coupled motion of 1L and 2L involves the contacts made by the linker helices that extend from the γ-phosphate-binding site (in the R portion) to 1L and 2L, in accord with the suggestion of Roseman *et al*. (12). When ATP binds to the trans ring, the inverse motion is expected to occur, as shown in the right-hand diagram of Fig. 4*c*.

DISCUSSION

The conformational dynamics of the molecular chaperonin GroEL have been studied by normal mode analyses of the individual subunits and a key multisubunit construct in the absence and presence of the allosteric effector ATP. The results demonstrate that the structure of the individual subunits has evolved to facilitate the motions (hinge bending and twisting at domain interfaces) required for the GroEL cycle. The large-scale tertiary structural change induced by ATP binding in the individual subunits appears to be a primary source of the positive cooperativity within a ring because steric repulsions would arise if one subunit changed its conformation and its neighbors did not. Thus, coupled tertiary structural changes of the subunits, rather than a quaternary structural transition, are involved in the observed cooperativity of ATP binding. The interring allosteric coupling is dominated by the motion of the equatorial domains. The normal mode results for three coupled equatorial domains show how the displacement of a domain in the cis ring associated with ATP binding can induce complementary motions of the two trans ring domains in contact with it. This is a source of negative cooperativity between the rings.

Although many elements of the structural transitions and their role in allosteric communication in the GroEL cycle now have been elucidated, a complete description of this complex system requires further analysis. The availability of structures for the end states (14–17) should make it possible to determine a detailed reaction path (43) for the allosteric mechanism of what has been characterized as a "two-stroke motor" (44).

We thank Paul Sigler for helpful discussions and comments on the manuscript. We thank Erik Evensen for assistance with the graphics. This work is supported in part by a grant from the National Institutes of Health. J.M. was the recipient of a postdoctoral fellowship from Burroughs Wellcome Fund Program in Mathematics and Molecular Biology during early stages of the work. He is now a postdoctoral fellow of the National Institutes of Health. Many of the calculations were done on the SGI Power Challenge at the National Center for Supercomputing Applications (NCSA) under a grant from the National Science Foundation. We thank the NCSA personnel for their help.

1. Ellis, R. J. & van der Vies, S. M. (1991) *Annu. Rev. Biochem.* **60,** 321–347.
2. Gething, M. J. & Sambrook, J. (1992) *Nature (London)* **355,** 33–45.
3. Corrales, F. J. & Fersht, A. R. (1996) *Proc. Natl. Acad. Sci. USA* **93,** 4509–4512.
4. Hartl, F. U. (1996) *Nature (London)* **381,** 571–580.
5. Clarke, A. R. (1996) *Curr. Opin. Struct. Biol.* **6,** 43–50.
6. Martin, J. & Hartl, F. U. (1997) *Curr. Opin. Struct. Biol.* **7,** 41–52.
7. Fenton, W. A. & Horwich, A. L. (1997) *Protein Sci.* **6,** 743–760.
8. Gray, T. E. & Fersht, A. R. (1991) *FEBS Lett.* **292,** 254–258.
9. Bochkareva, E. S., Lissin, N. M., Flynn, G. C., Rothman, J. E. & Girshovich, A. S. (1992) *J. Biol. Chem.* **267,** 6796–6800.
10. Jackson, G. S., Staniforth, R. A., Halsall, D. J., Atkinson, T., Holbrook, J. J., Clarke, A. R. & Burston, S. G. (1993) *Biochemistry* **32,** 2554–2563.
11. Chen, S., Roseman, A. M., Hunter, A. S., Wood, S. P., Burston, S. G., Ranson, N. A., Clarke, A. R. & Saibil, H. R. (1994) *Nature (London)* **371,** 261–264.
12. Roseman, A. M., Chen, S., White, H., Braig, K. & Saibil, H. (1996) *Cell* **87,** 241–251.
13. Llorca, O., Marco, S., Carrascoua, J. L. & Valpuesta, J. M. (1997) *J. Struct. Biol.* **118,** 31–42.
14. Xu, Z., Horwich, A. L. & Sigler, P. B. (1997) *Nature (London)* **388,** 741–750.
15. Braig, K., Otwinowski, Z., Hegde, R., Boisvert, D. C., Joachimiak, A., Horwich, A. L. & Sigler, P. B. (1994) *Nature (London)* **371,** 578–586.
16. Braig, K., Adams, P. D. & Brünger, A. T. (1995) *Nat. Struct. Biol.* **2,** 1083–1094.
17. Boisvert, D. C., Wang, J., Otwinowski, Z., Horwich, A. L. & Sigler, P. B. (1996) *Nat. Struct. Biol.* **3,** 170–177.
18. Brooks, B. R. & Karplus, M. (1985) *Proc. Natl. Acad. Sci. USA* **82,** 4995–4999.
19. Harrison, R. W. (1984) *Biopolymers* **23,** 2943–2949.
20. Marques, O. & Sanejouand, Y. H. (1995) *Proteins* **23,** 557–560.
21. Monawad, L. & Perahia, D. (1996) *J. Mol. Biol.* **258,** 393–410.
22. Thomas, A., Field, M. J. & Perahia, D. (1996) *J. Mol. Biol.* **261,** 490–506.
23. Brooks, C. L., Karplus, M. & Pettitt, B. M. (1988) *Adv. Chem. Phys.* **71,** 1–249.
24. Brooks, B. R., Janežic, D. & Karplus, M. (1995) *J. Comp. Chem.* **16,** 1522–1542.
25. Brooks, B. R., Bruccoleri, R. E., Olafson, B. D., States, D. J., Swaminathan, S. & Karplus, M. (1983) *J. Comp. Chem.* **4,** 187–217.
26. Brooks, B. R. & Karplus, M. (1983) *Proc. Natl. Acad. Sci. USA* **80,** 6571–6575.
27. White, H. E., Chen, S., Roseman, A. M., Yifrach, O., Horovitz, A. & Saibil, H. R. (1997) *Nat. Struct. Biol.* **4,** 690–694.
28. Zeilstra-Ryalls, J., Fayet, O. & Georgopoulos, C. (1994) *J. Bacteriol.* **176,** 6558–6565.
29. Lorimer, G. H. & Todd, M. J. (1995) *Nat. Struct. Biol.* **2,** 1083–1094.
30. Rye, H. S., Burston, S. G., Fenton, W. A., Beechem, J. M., Xu, Z., Sigler, P. B. & Horwich, A. L. (1997) *Nature (London)* **388,** 792–798.
31. Hayer-Hartl, M. K., Weber, F. & Hartl, F. U. (1996) *EMBO J.* **15,** 6111–6121.
32. Yifrach, O. & Horovitz, A. (1994) *J. Mol. Biol.* **243,** 397–401.
33. Yifrach, O. & Horovitz, A. (1995) *Biochemistry* **34,** 5303–5308.
34. Monod, J., Wyman, J. & Changeux, J. P. (1965) *J. Mol. Biol.* **12,** 88–118.
35. Perutz, M. F. (1970) *Nature (London)* **228,** 726–734.
36. Gelin, B. R., Lee, A. W.-M. & Karplus, M. (1983) *J. Mol. Biol.* **171,** 489–559.
37. Lee, A. W.-M. & Karplus, M. (1983) *Proc. Natl. Acad. Sci. USA* **80,** 7055–7059.
38. Yifrach, O. & Horovitz, A. (1996) *J. Mol. Biol.* **255,** 356–361.
39. Murai, N., Makino, Y. & Yoshida, M. (1996) *J. Biol. Chem.* **271,** 28229–28234.
40. Zahn, R., Buckle, A. M., Perrett, S., Johnson, C. M., Corrales, F. J., Golbik, R. & Fersht, A. R. (1996) *Proc. Natl. Acad. Sci. USA* **93,** 15024–15029.
41. Altamirano, M. M., Golbik, R., Zahn, R., Buckle, A. M. & Fersht, A. R. (1997) *Proc. Natl. Acad. Sci. USA* **94,** 3576–3578.
42. Buckle, A. M., Zahn, R. & Fersht, A. R. (1997) *Proc. Natl. Acad. Sci. USA* **94,** 3571–3575.
43. Ma, J. & Karplus, M. (1997) *Proc. Natl. Acad. Sci. USA* **94,** 11905–11910.
44. Lorimer, G. (1997) *Nature (London)* **388,** 720–723.
45. Kraulis, P. J. (1991) *J. Appl. Crystallogr.* **24,** 946–950.
46. Merritt, E. A. & Murphy, M. E. P. (1994) *Acta Crystallogr. D* **50,** 869–873.